23rd Australasian Fluid Mechanics Conference - 23AFMC
Sydney, Australia
4 – 8 December 2022
Paper No: AFMC2022-178

Large Eddy Simulation of Artificially Generated Atmospheric Vortices for Power Generation

T. Bischof[1*], M. MacDonald[1], J. E. Cater[2], and R. G. J. Flay[1]

[1] Department of Mechanical and Mechatronics Engineering, The University of Auckland, Auckland, New Zealand
[2] Department of Engineering Science, The University of Auckland, Auckland, New Zealand
*mailto: tbis544@aucklanduni.ac.nz

Abstract

A numerical simulation of atmospheric buoyancy vortices for power generation is conducted using the Large Eddy Simulation (LES) method. Vanes, for generating a swirl, and a turbine, for extracting torque, are modelled using a body-forcing momentum source and sink method, respectively. Only minor changes in the vortex structure are visible when the turbine is present. Furthermore, the low velocities lead to an insignificantly small torque on the turbine. The so-called vortex wandering effect is observed for all cases simulated. Models without the turbine and changes in heat source location are further investigated to analyse the maximum radius and distribution of the vortex wandering. Overall, the modelling of vanes and the turbine as momentum source and sink leads to a significant reduction in computational time compared to simulations containing solid, resolved geometries.

1 Introduction

Higher energy demands and climate change concerns have been a motivation for the growth of new renewable energy technologies. One of these renewable substitutes is implementing artificially generated vortices (Mustafa 2015, Ismaeel 2017). Dust-devil-like vortices are naturally occurring phenomena in the atmospheric boundary layer that can be perceived as heat engines that convert heat into mechanical energy (Renno *et al.* 1998). Little has been published on the actual availability of energy in vortices. Michaud *et al.* (1999) proposed the idea of capturing mechanical energy from controlled tornado-like vortices with an Atmospheric Vortex Engine (AVE). Das *et al.* (2020) used a computational fluid dynamics model to investigate the Solar Vortex Engine (SVE). Solar Vortex Engine plants capture solar energy with solar collectors to generate the buoyant updraft in a vortex, whereas the AVE uses waste heat energy. It was found that the efficiency of the technology is low due to its limitation in size, and also, a larger numerical model with more realistic atmospheric conditions is required to reach a commercialisation stage (Das 2020).

The work discussed in this paper is part of a large research programme focused on understanding how to artificially generate buoyancy vortices using waste heat that is anchored to the location of the waste heat source. The research programme uses a three-pronged attack, combining computational fluid dynamics (CFD), laboratory-based experiments, and theoretical analysis in order to gain an understanding of buoyancy vortices. The outcome of this understanding will be incorporated into the design of a demonstration vortex engine to be built in New Zealand. The aspect considered in this paper is part of the CFD programme aimed at developing methods to simply model both the swirl vanes, which rotate the incoming flow to the vortex near the ground and the turbine, which extracts angular momentum from the flow to produce torque. Modelling both the vanes and turbine similar to an actuator-disk model is being explored, as they have the potential to execute much faster

than if multiple individual swirl vane foils and turbine blades are implemented. This faster execution will then enable the effect of swirl vane and turbine design features on the strength of the vortex to be investigated efficiently. The overall objective is to find the required characteristics to maximise the power output for a particular vortex. Then, for example, knowing the torque and pressure drop coefficients from this study, the required turbine design features, such as the number of blades, can be determined for the design.

2 Methodology

2.1 Computational Domain and Model

The study has been carried out using an anelastic Large Eddy Simulation (LES) model in OpenFOAM. The computational domain is a cylinder with a radius of 25 m and a height of 150 m. An orthogonal grid system is chosen with stretching in the radial and vertical directions. No extensive grid sensitivity study has been carried out at this stage, but a finer mesh did show quantitatively similar plots to Figure 2. The heat source, which represents the waste heat, is modelled as a cylinder in which air entering it is heated up to a temperature of 60 °C. It is placed in the centre of the domain with a radius of 0.36 m, a height of 4 m and with the lower edge at the ground level. The LES method with the dynamic Smagorinsky subgrid-scale (SGS) model is used as the turbulence model. The wall functions are based on the Monin–Obukhov similarity theory implemented in a similar manner to the SOWFA (Simulator fOr Wind Farm Applications) solver, which has been successfully applied in a range of atmospheric boundary layer studies (Fleming *et al.* 2014, Martinez-Tossas *et al.* 2018).

The numerical model simulates the atmosphere under the anelastic approximation (Bannon 1996), in which pressure, density and potential temperature are defined with a base state which only varies with height and a fluctuation, or perturbation, of the base state, which is solved for. These changes with height lead to more realistic atmospheric conditions compared to the standard solvers with the Boussinesq approximation (Bannon 1996). The sides and the top boundary conditions are set as either zero gradients, inlet-outlet coupled or total hydrostatic pressure. This allows for a natural outflow of the vortex at the top while using ambient atmospheric conditions for inflows into the domain. The boundary conditions of the ground surface are either set to atmospheric boundary layer wall functions or zero gradients.

2.2 Modelling of Vanes and Turbine

The vanes and the turbine are important elements of the atmospheric vortex engine technology. When added to the numerical model as solid parts, a very fine unstructured mesh around the surfaces would be required, which leads to computational complexity and an increase in run time. To overcome this issue, the vanes and the turbine are numerically modelled as momentum source and sink with a similar approach to an actuator disk model. Figure 1(a) shows the cell sets of the vanes, turbine, and heat source within the domain. The vane cell set ring is placed at a radius of around 5 m, with a cell thickness of around 0.2 m and a total height of 3 m. The turbine cell set ring has a height of 0.25 m, a radius of around 0.5 m with a cell thickness of around 0.05 m. The origin of the axis is located at the centre of the turbine. A schematic plan of the vanes and turbine implementation is shown in Figure 1(b).

The vanes are implemented as a force that is applied to the incoming air and deflects the flow in the desired direction. To achieve that, a new source term in the form of a pressure gradient $\nabla P_v(i)$ has been added to the momentum equation, which uniformly directs the incoming flow (upstream velocity) in the direction of the vanes. In this study, the direction is set to 45 ° to the centripetal axis. The directional pressure gradient for each cell is calculated using Equation (1), where $A(i,i)$ is the

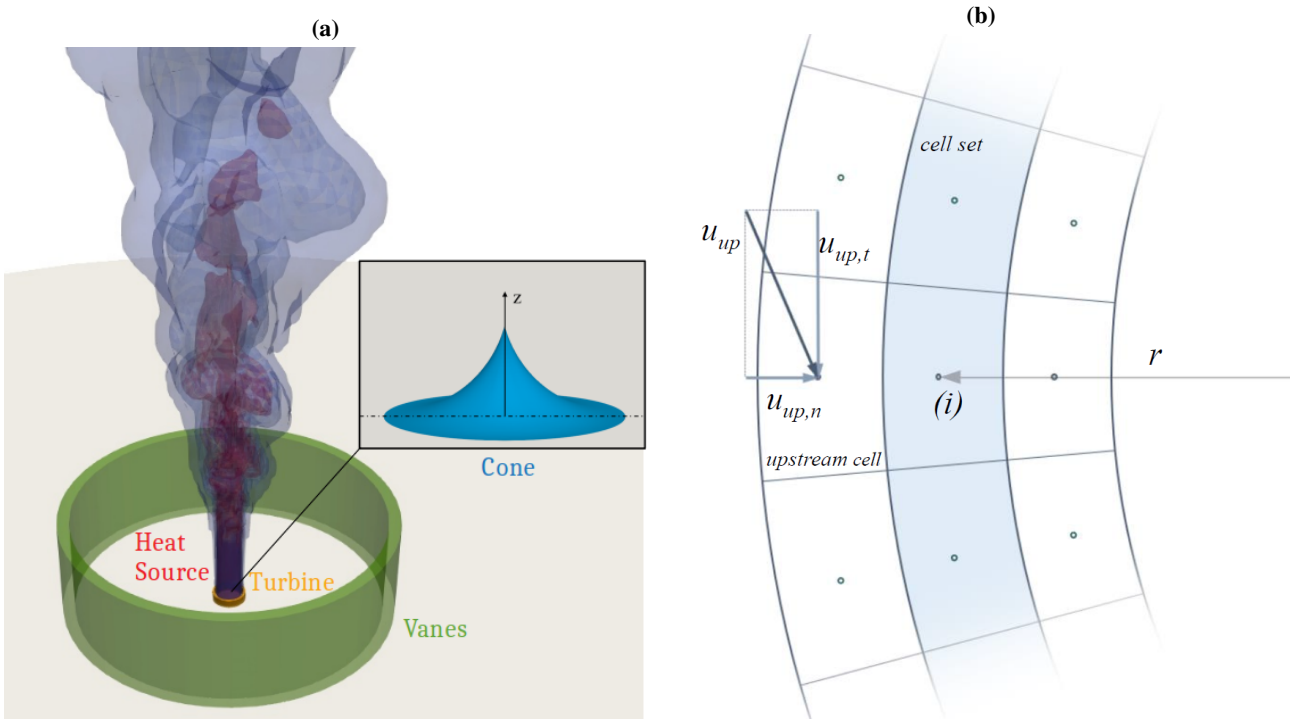

Figure 1. a) Computational domain with cell sets, and b) a schematic of the vanes and turbine implementation, where the blue region is either the vanes or the turbine. The cone is only used in one case, see Section 2.3

diagonal term of discretisation matrix A, $D(i)$ is the rotation matrix of the upstream velocity in the desired flow direction, $u_{up}(i)$ is the upstream velocity, and $u(i)$ is the cell velocity. The variable i is the cell index of the cell set corresponding to the vanes.

$$\nabla P_v(i) = A(i,i)[D(i) \cdot u_{up}(i) - u(i)] \tag{1}$$

A similar but distinct approach is applied to consider a turbine ring's presence. For the turbine cells, a sink is added to the momentum equation consisting of the sum of a force in the tangential direction $F_t(i)$ and a force in the normal direction $F_n(i)$. The tangential force for each cell is calculated using the torque over the cell centre radius, $F_t(i) = T(i)/r$. The normal force is calculated using the pressure drop in the normal direction times the cross-sectional area of the cell, $F_n(i) = dP(i) \times A(i)$.

The torque at each turbine cell is acting in the tangential direction and is defined using Equation (2), where $\rho(i)$ is the density at the cell, h is the turbine height, $u_{up,t}(i)$ is the tangential component of the upstream velocity, N is the number of cells in the set, and r_{out} is the outer radius of the turbine cell ring. At the current stage, the torque coefficient C_t is conditional on the turbine's rotational speed, efficiency, and incoming flow. However, this relationship needs to be further explored.

$$T(i) = \underbrace{\frac{1}{2}\rho(i)\,u_{up,t}(i)^2}_{dynamic\ pressure} \times \underbrace{\frac{2\pi r_{out}\,h}{N}}_{reference\ area} \times \underbrace{r_{out}}_{reference\ length} \times \underbrace{C_t}_{torque\ coefficient} \tag{2}$$

The change in the normal direction is defined with the pressure difference, which is calculated using Equation (3), where $u_{up,n}(i)$ is the normal component of the upstream velocity and C_p is the pressure coefficient.

$$dP(i) = C_p \times 0.5 \times \rho(i) \times u(i)^2_{up,n} \tag{3}$$

The resulting turbine power $W(i)$ is calculated using Equation (4) with C_w being the power coeffi-

cient. Similar to the torque coefficient, the power coefficient depends on the rotational speed, turbine efficiency, and incoming velocity.

$$W(i) = \underbrace{\frac{1}{2}\rho(i)\,u_{up,n}(i)^2}_{dynamic\ pressure} \times \underbrace{\frac{2\pi\, r_{out}\, h\, u_{up,n}(i)}{N}}_{volume\ \ flow\ rate} \times \underbrace{C_w}_{power\ coefficient} \tag{4}$$

The torque and the power are calculated at each turbine cell and summed to get the total torque and power of the turbine. The equations are based on the Euler equations, which relate the change in angular momentum of a flow field to the torque on an impeller (White 2017). Turbine model assumptions include inviscid, homogeneous, and incompressible flow in the area of interest.

2.3 Case Description

A variety of atmospheric vortex models are investigated. The initial study is conducted without the presence of the turbine ring and with the heat source on the ground. This initial study is chosen to provide a reference case of an unaltered vortex in which rotational energy is extracted by a turbine. For the next several cases, the turbine model is added with varying torque coefficient C_t to analyse the impact of the turbine's existence on the vortex structure. For the last study, the turbine is removed to investigate the wandering of the vortex. Three cases with different heat source locations are considered. The heat source in the first case is placed on the ground. For the second case, the heat source is a 10m-high volume placed at 1 m above the ground. The heat source represents hot water sprayed into the air, where the hot water evaporates into water vapour, saturating the air as well as warming the air volume. Placing the heat source in the air is an arrangement that protects the turbine blades by minimising the water droplets going through the turbine. Lastly, the heat source is at the same location as the second case but with a curved cone placed in the centre below to help direct the flow from horizontal to vertical. The curved cone has dimensions of a height of 0.25 m and a radius of 0.3 m (Figure 1).

3 Results and Discussion

3.1 Domain Without Turbine

Time-averaged vertical profiles of the vertical velocity, the potential temperature, and the pressure are presented in Figure 2. The case is an initial study without the turbine and with a heat source placed from the ground level up to 4 m height. The data have been sampled at the centre line of the domain, which nominally represents the centre of the atmospheric vortex, and averaged over time. The vertical velocity w (Figure 2(a)) peaks at around 3.7 m/s above the heat source and then decreases with height as the vortex decays. A notable drop in the vertical velocity is seen at the top of the domain, which is due to the plume diffusing. Likewise, the potential temperature θ (Figure 2(b)) starts cooling down immediately above the heat source where entrainment with the ambient air arises. Figure 2(c) displays the pressure term p/ρ changing with height where a fluctuation above the heated volume indicates the interaction with the surrounding air.

Figure (3) shows two time-averaged horizontal transects, at 5 m above the ground (Figure 3(a)) and 10 m above the ground (Figure 3(b)). The velocity profiles and the pressure drop above the heat source at 5 m height are similar in shape to what can be seen in the study of dust-devil-like vortices by Raasch & Franke (2011). Their study shows a steeper change in potential temperature at the core centre. The main reason for the different profile shapes is the local heat source in this case compared to the uniform ground heating in Raasch & Franke (2011). When comparing the 10 m to the 5 m profiles, the decay of the vortex is visible, as all the profiles flatten out in the horizontal direction.

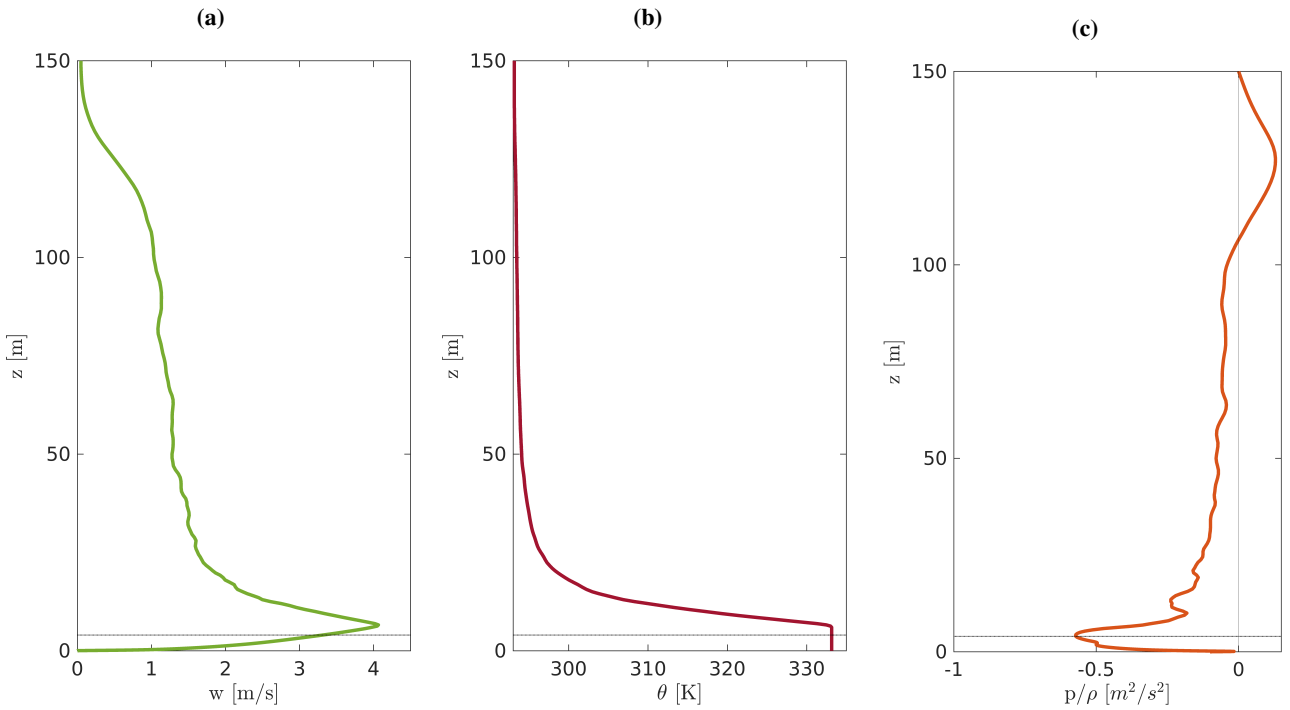

Figure 2. Time-averaged vertical profiles for a) the vertical velocity w, b) the potential temperature θ, and c) the pressure p/ρ at the domain centre line. The horizontal line denotes the top of the heat source.

Although some physical properties have a similar shape and are qualitatively comparable, the scales are quite different, which is also related to the choice of heat source. The results indicate that the model is accurately capturing the vortex.

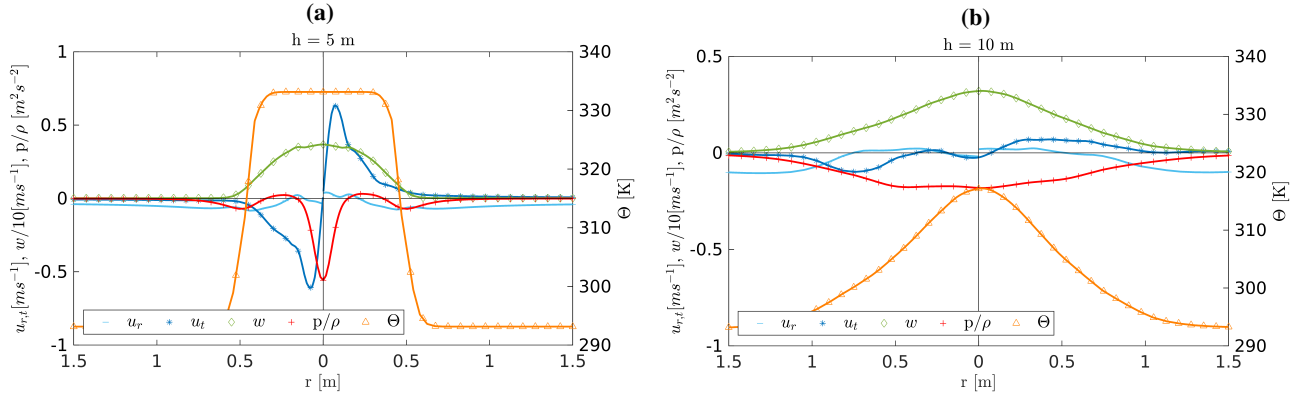

Figure 3. Time-averaged horizontal transects at a) 5 m and b) 10 m, showing the radial u_r, tangential u_t, and vertical w velocities, as well as the pressure p/ρ and the potential temperature θ. The vertical velocity w is divided by 10 to fit the scale (left).

3.2 Domain including Turbine Model

We now add the turbine into the domain and systematically vary the torque coefficient C_t in Equation (2) from 0 to 90 while keeping the pressure coefficient C_p in Equation (3) constant at 0.7. It was found that the turbine momentum-sink model results in a minor reduction of tangential velocity. However, the changes are very small and only visible for high C_t values (≥ 9) due to very low incoming velocities. As the torque (Equation (2)) is scaled by the incoming tangential velocity squared, the resulting force is minor, and no significant change in the vortex structure is apparent (not shown). In

general, the results show that the turbine model is working, but it will require further improvement to understand the relationship between the coefficients, the velocities and the torque.

Note that moving the heat source up in the air, compared to the previous localised ground heating, seems to complicate the modelling of the turbine sink. Placing the heat volume source 1 m above the ground caused disturbance close to the ground and downward flow below the heat source, and outwards flow from the domain centre across the turbine. This flow circulation interacted with the turbine model and caused unreasonable results, for instance, adding momentum and forcing the air inside the turbine to flow out of the centre.

Overall, a reduction of 10^2 mesh cells (4 days to less than 12 hrs run time) is achieved by only modelling the vanes as a momentum source (Bischof *et al.* 2020). For that reason, it is advantageous to model the turbine as a momentum sink similar to existing techniques like an actuator disk model.

3.3 Vortex Wandering

The wandering of vortices has been observed in various studies, for instance, Ashton *et al.* (2019) and Verma & Selvam (2020). The wandering in this set-up is investigated without the presence of the turbine model to capture the maximum distance the vortex wanders away from the centre. The heat source is placed at the ground for the case presented in Figure 4.

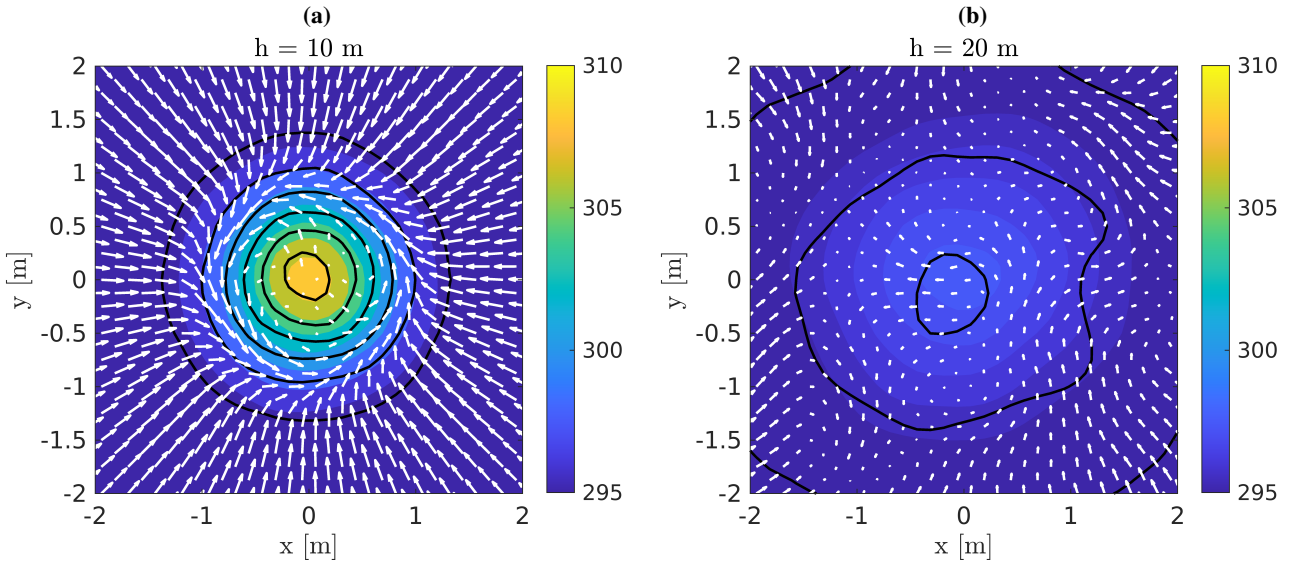

Figure 4. Time-averaged horizontal cross-sections of potential temperature θ at (a) 10 m height and (b) 20 m height. The contour lines refer to the pressure p/ρ ranging from -0.3 to -0.05 m^2/s^2 at intervals of 0.05 m^2/s^2. Velocity vectors are added to the contour plots.

The time-averaged vorticity is shown on two horizontal planes in Figure 4, (a) at 10 m and (b) at 20 m. At a lower level, we can see that there is mainly radial inflow and not much swirl left from the vanes, which are placed at a 5 m radius. But this cross-section shows that around a radius of 1 m vorticity seems to develop and forms the vortex above the heat source. Figure 4(a) is also very symmetric, whereas, at 20 m height, this symmetry seems to vanish. The small local vorticity arising at 20 m above the ground was also noticed by Verma & Selvam (2020), and they stated it was due to the decrease in local swirl ratios.

For the distance wandering of the core, three cases described in the methodology are investigated. For the first case, Figure 5(a) shows the minimum pressure locations at three heights for every 0.5 s and a period of 400 s simulation time. Only minimum pressure locations for vorticity ≥ 0.5 s^{-1} are considered, which represents the vortex core mentioned by Raasch & Franke (2011). From the histogram, it is possible to observe that the vortex at 10 m height wanders within a lot smaller radius

than at 100 m height. Not only is the radius a lot smaller, the wandering also has the form of a Gaussian distribution which flattens with height. Fewer minimum pressure locations are visible with height due to the decrease in vorticity and the wandering far away from the domain centre out of the presented display window.

The second and third cases have a very similar distribution, the main difference is that the vortex seems to decay and wander out of the centre faster with height if there is no cone. This can be seen in Figure 5(b) and Figure 5(c), where significantly fewer minimum pressure locations are visible for the latter case. The cone seems to be strengthening and centring the vortex with height.

Placing the heat source at the ground did not impact the wandering of the vortex with height, but it avoided the swirling flow below the heat source, which forced the air outflow across the turbine surface (Section 3.2).

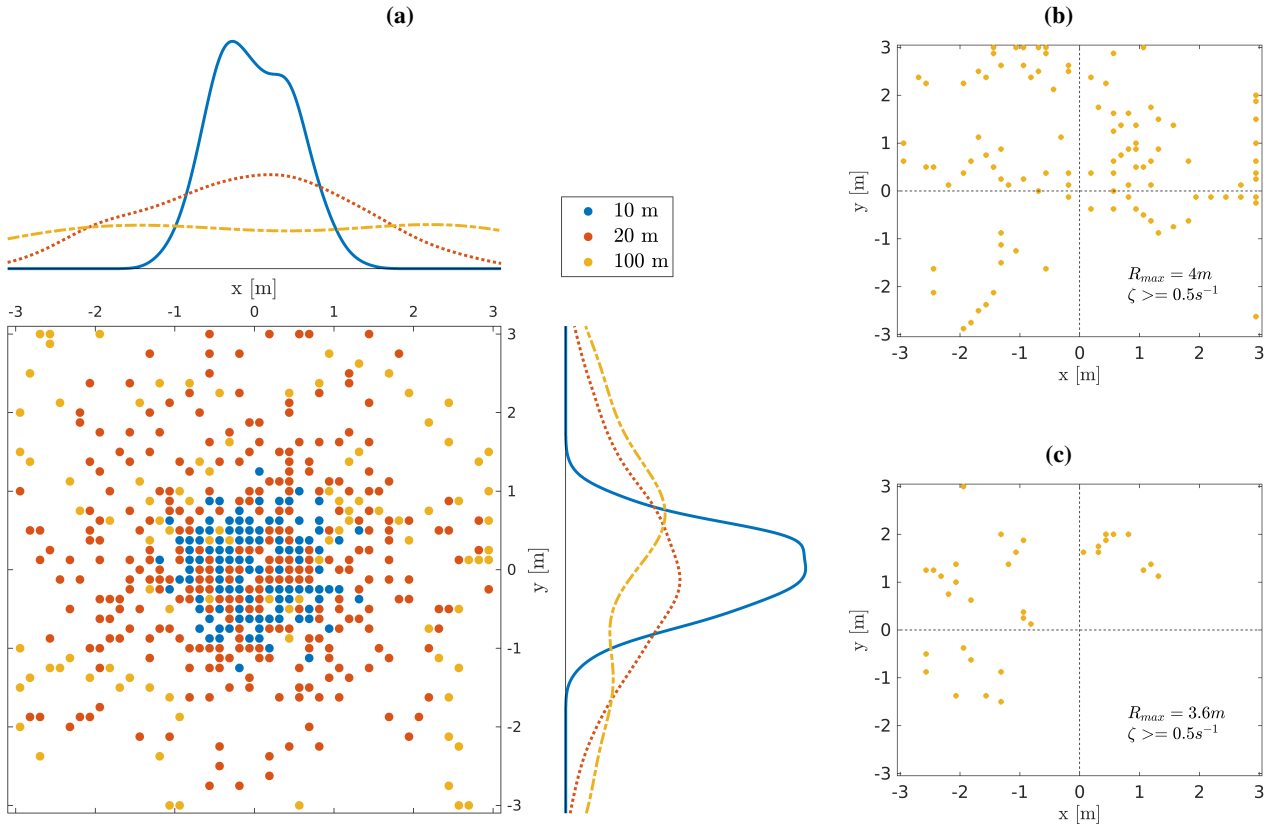

Figure 5. Scatter plot of instantaneous vortex core location for a) the case without the cone and heat source on the ground. Three heights are shown, including a histogram. In addition, the scatter plots at 100 m above ground for the cases with the heat source in the air, b) including the cone, and c) without the cone.

4 Conclusions

Artificially generated buoyancy vortices have been created using a heated volume of air as the energy source located inside a ring of swirl vanes. The effect of the ring of individual swirl vanes on the airflow has been modelled, which is able to impart angular momentum to the flow such that the incoming flow from the vanes is in a user-specified direction, e.g. at 45° to the radial direction.

A model for the impact of the turbine presence is also presented. In this case, the angular momentum applied to the incoming flow is specified by torque and pressure coefficients. In the test case with a heat source between the ground and a height of 4 m and without a turbine, both the vertical component of velocity and the potential temperature falls rapidly at the height above the heat source.

Horizontal transects across the vortex (without a turbine) show velocity profiles that are similar in shape to those seen by others in studies of dust devils (Raasch & Franke 2011). Estimates of turbine power are very small, as expected given the small power of the heat source, but the results show that the turbine model is working. A compelling reduction of 10^2 mesh cells is achieved by only modelling the vanes as a momentum source, and a significantly lower computational time is achieved by modelling the turbine as a momentum sink.

The developed vortex has been observed to wander, and as expected, this wandering increases with an increase in height. The presence of a cone at the centre of the turbine strengthened and helped to centre the vortex compared to having no cone present.

Acknowledgements

The authors acknowledge the financial support from the Royal Society Te Apārangi of New Zealand for the Marsden Fund Grant 18-UOA-013. The authors also acknowledge the New Zealand eScience Infrastructure (NeSI) high-performance computing facilities used in this research.

References

Ashton, R., Refan, M., Iungo, G. V., and Hangan, H., 2019, Wandering corrections from PIV measurements of tornado-like vortices, *J. Wind Eng. Ind. Aerod.*, **189**, 163–172.

Bannon, P. R., 1996, On the Anelastic Approximation for a Compressible Atmosphere, *J. Atmos. Sci*, **53**, 3618–3628.

Bischof, T., MacDonald, M., Cater, J. E., and Flay, R. G. J., 2020, Numerical Simulations of Laboratory-Scale Buoyancy Vortices, *AFMC2020, Brisbane, Australia*.

Das, P., and Chandramohan, V. P., 2020, Estimation of flow parameteres and power potential of solar vortex engine (SVE) by varying its geometrical configuration: A numerical study, *Energy Convers. Manag*, **223**, 113272-1–16.

Martinez-Tossas, L. A., Churchfield, M. J., Yilmaz, A. E., Sarlak, H., Johnson, P. L., Sorensen, J. N., Meyers, J. and Meneveau, C., 2018, Comparison of four large-eddy simulation research codes and effects of model coefficient and inflow turbulence in actuator-line-based wind turbine modeling, *J. Renew. Sustain. Energy*, **10**, 033301-1–12.

Michaud, L. M., 1999, Vortex process for capturing mechanical energy during upward heat-convection in the atmosphere, *J. Appl. Energy*, **62**, 241–251.

Mustafa, A. T., Al-Kayiem, H. H., and Gilani, S. I. U., 2015, A review of convective and artifical vortices for power generation, *Int. J. Sus. Dev. Plann.*, **10(5)**, 650–665.

Fleming, P. A., Gebraad, P. M. O., Lee, S., van Wingerden, J., Johnson, K., Churchfield, M., Michalakes, J., Spalart, P., and Moriarty, P., 2014, Evaluating techniques for redirecting turbine wakes using SOWFA, *Renew. Energy*, **70**, 211–218.

Ismaeel, A. A., Al-Kayiem, H. H., Baheta, A. T. and Aurybi, M. A., 2017, Review and comparative analysis of vortex generation systems for sustainable electric power production, *IET Renew. Power Gener.*, **11(13)**, 1613–1624.

Raasch, S. and Franke, T., 2011, Structure and formation of dust devil–like vortices in the atmospheric boundary layer: A high-resolution numerical study, *J. Geophys. Res.*, **116**, D16120-1–16.

Renno, N. O., Burkett, M. L. and Larkin, M. P., 1998, A Simple Thermodynamical Theory for Dust Devils, *J. Atmos. Sci*, **55**, 3244–3252.

Verma, S., and Selvam, R. P., 2020, CFD to VorTECH Pressure-Field Comparison and Roughness Effect on Flow, *J. Struct. Eng*, **146(9)**, 04020187-1–12.

White, M. F., 2017, *Fluid Mechanics (8th edition)*, Boston, Mass: WCB/McGraw-Hill.